SINTEF
PROCEEDINGS
1

Selected papers from 10th International Conference on Computational Fluid Dynamics in the Oil & Gas, Metallurgical and Process Industries

Progress in Applied CFD

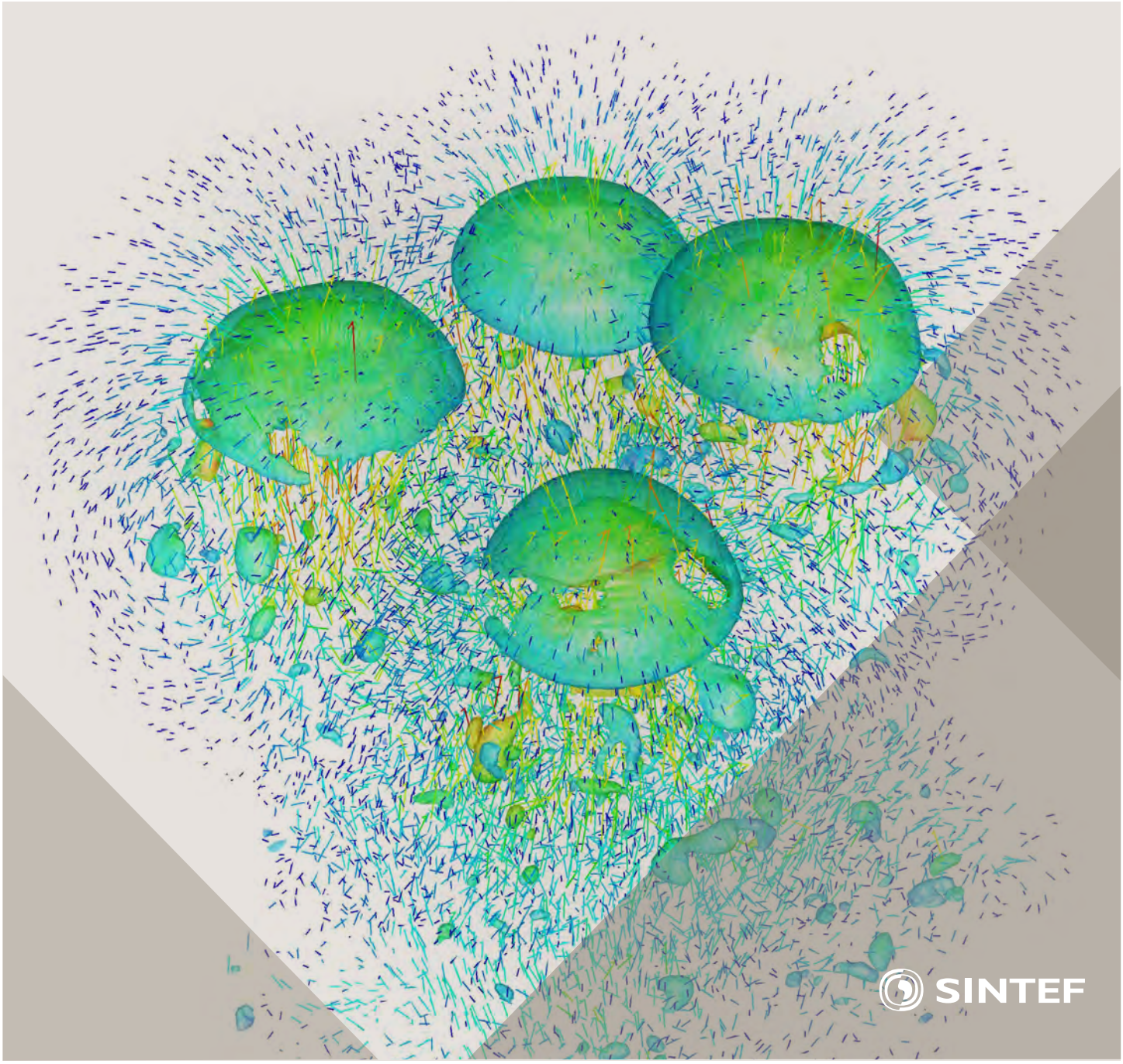

SINTEF Proceedings

Editors:
Jan Erik Olsen and Stein Tore Johansen

Progress in Applied CFD

Selected papers from 10th International Conference on Computational Fluid Dynamics in the Oil & Gas, Metallurgical and Process Industries

SINTEF Academic Press

SINTEF Proceedings no 1
Editors: Jan Erik Olsen and Stein Tore Johansen
Progress in Applied CFD
Selected papers from 10th International Conference on Computational Fluid Dynamics in the Oil & Gas, Metallurgical and Process Industries

Key words:
CFD, Flow, Modelling

Cover, illustration: Rising bubbles by Schalk Cloete

ISSN 2387-4287 (printed)
ISSN 2387-4295 (online)
ISBN 978-82-536-1432-8 (printed)
ISBN 978-82-536-1433-5 (pdf)

60 copies printed by AIT AS e-dit
Content: 100 g munken polar
Cover: 240 g trucard

SINTEF Academic Press
Address: Forskningsveien 3 B
PO Box 124 Blindern
N-0314 OSLO
Tel: +47 22 96 55 55
Fax: +47 22 96 55 08

www.sintef.no/byggforsk
www.sintefbok.no

SINTEF Proceedings
SINTEF Proceedings is a serial publication for peer-reviewed conference proceedings on a variety of scientific topics.
The processes of peer-reviewing of papers published in SINTEF Proceedings are administered by the conference organizers and proceedings editors. Detailed procedures will vary according to custom and practice in each scientific community.

PREFACE

This book contains selected papers from the 10th International Conference on Computational Fluid Dynamics in the Oil & Gas, Metallurgical and Process Industries. The conference was hosted by SINTEF in Trondheim in June 2014 and is also known as CFD2014 for short. The conference series was initiated by CSIRO and Phil Schwarz in 1997. So far the conference has been alternating between CSIRO in Melbourne and SINTEF in Trondheim. The conferences focus on the application of CFD in the oil and gas industries, metal production, mineral processing, power generation, chemicals and other process industries. The papers in the conference proceedings and this book demonstrate the current progress in applied CFD.

The conference papers undergo a review process involving two experts. Only papers accepted by the reviewers are presented in the conference proceedings. More than 100 papers were presented at the conference. Of these papers, 27 were chosen for this book and reviewed once more before being approved. These are well received papers fitting the scope of the book which has a slightly more focused scope than the conference. As many other good papers were presented at the conference, the interested reader is also encouraged to study the proceedings of the conference.

The organizing committee would like to thank everyone who has helped with paper review, those who promoted the conference and all authors who have submitted scientific contributions. We are also grateful for the support from the conference sponsors: FACE (the multiphase flow assurance centre), Total, ANSYS, CD-Adapco, Ascomp, Statoil and Elkem.

Stein Tore Johansen & Jan Erik Olsen

Organizing committee:

Conference chairman: Prof. Stein Tore Johansen
Conference coordinator: Dr. Jan Erik Olsen
Dr. Kristian Etienne Einarsrud
Dr. Shahriar Amini
Dr. Ernst Meese
Dr. Paal Skjetne
Dr. Martin Larsson
Dr. Peter Witt, CSIRO

Scientific committee:

J.A.M.Kuipers, TU Eindhoven
Olivier Simonin, IMFT/INP Toulouse
Akio Tomiyama, Kobe University
Sanjoy Banerjee, City College of New York
Phil Schwarz, CSIRO
Harald Laux, Osram
Josip Zoric, SINTEF
Jos Derksen, University of Aberdeen
Dieter Bothe, TU Darmstadt
Dmitry Eskin, Schlumberger
Djamel Lakehal, ASCOMP
Pär Jonsson, KTH
Ruben Shulkes, Statoil
Chris Thompson, Cranfield University
Jinghai Li, Chinese Academy of Science
Stefan Pirker, Johannes Kepler Univ.
Bernhard Müller, NTNU
Stein Tore Johansen, SINTEF
Markus Braun, ANSYS

CONTENTS

10th International Conference on CFD in Oil & Gas, Metallurgical and Process Industries
SINTEF, Trondheim, Norway *CFD 2014*
17-19 June 2014

The parametric sensitivity of fluidized bed reactor simulations carried out in different flow regimes

Schalk CLOETE*, Jan H. CLOETE, Stein Tore JOHANSEN & Shahriar AMINI

[1] SINTEF Materials and Chemistry, 7465 Trondheim, NORWAY

* E-mail: schalk.cloete@sintef.no

ABSTRACT

Fluidized bed simulations carried out within the Kinetic Theory of Granular Flows framework utilize a number of model coefficients which are strongly case dependent and difficult to determine accurately. The most important of these are the specularity coefficient (the degree of friction at the wall) and the particle-particle restitution coefficient (inelasticity of inter-particle collisions). This paper demonstrated that modification of these coefficients can trigger a regime change in very narrow and fast risers, thereby introducing a great amount of uncertainty. For situations sufficiently far from the dilute transport regime, however, sudden regime changes were not observed and the influence of these unknown parameters is more systematic. It was shown that in the case of wide bubbling beds, the effect of these unknown model coefficients can become negligible, making these reactors attractive for simulation studies. Faster and narrower geometries, on the other hand, exhibited greater sensitivity to changes in the specularity coefficient and particle-particle restitution coefficient, thereby introducing ever-increasing quantities of uncertainty stemming from these unknown model coefficients.

Keywords: Fluidized bed reactors, Two Fluid Model, Kinetic Theory of Granular Flows, Specularity coefficient, Restitution coefficient.

NOMENCLATURE

α	Volume fraction
ϕ	Damping of fluctuating motions [kg/(m.s^2)]
γ_{Θ_s}	Collisional dissipation rate [kg/(m.s^2)]
Θ	Granular temperature [m^2/s^2]
ρ	Density [kg/m^3]
$\bar{\bar{\tau}}$	Stress tensor [kg/(m.s^2)]
$\vec{\upsilon}$	Velocity vector [m/s]
∇	Gradient or Del operator [1/m]
C	Species concentration [mol/m^3]
d	Diameter [m]
$\vec{g}$	Gravity vector [m/s^2]
$\bar{\bar{I}}$	Identity tensor
K	Momentum exchange coefficient [kg/(m^3.s)]
k	Reaction rate constant
k_{Θ_s}	Granular temperature conductivity [kg/(m.s)]
p	Pressure [Pa]
Q	Volumetric flow rate [m^3/s]
R	Universal gas constant [kcal/(K.mol)]
R^H	Heterogeneous reaction rate [mol/(m^{3}s)]
S	Source term
T	Temperature [K]
t	Time [s]
V	Volume [m^3]
w	Solids weight [kg]
x	Mass fraction
Y	Species mass fraction

Sub/superscripts

$\vec{\upsilon}$	Momentum
g	Gas
i	Species index
sg	Inter-phase
s	Solids

INTRODUCTION

Fluidized bed reactors find application in a wide range of process industries, primarily due to their excellent gas-solid mass transfer and mixing characteristics. Despite these attractive advantages, however, these reactors are difficult to design and scale up due to the complex hydrodynamics of fluidization. Almost all types of fluidization are characterized by the formation of transient clusters of particles which can dominate transport phenomena inside the reactor. The behaviour of these clusters depends on a wide range of parameters and must be understood to ensure effective reactor design and scale-up.

With the continued exponential increase in computational power and availability, fundamental flow

modelling has emerged as a promising method for improving the understanding of the complex behaviour exhibited by fluidized bed reactors. The foremost of these modelling frameworks, the Two Fluid Model (TFM) closed by the Kinetic Theory of Granular Flows (KTGF) (Jenkins and Savage 1983, Lun, Savage et al. 1984, Gidaspow, Bezburuah et al. 1992, Syamlal, Rogers et al. 1993), has progressed to a high level of maturity over the past three decades of development and can already offer reliable predictions of fluidized bed behaviour (Taghipour, Ellis et al. 2005, Ellis, Xu et al. 2011, Cloete, Zaabout et al. 2014). It therefore holds great potential to support the design and accelerate the scale-up of fluidized bed reactor technology.

The primary challenge facing the TFM is the fine grids required to accurately resolve all of the small scale particle clusters. These fine grids make simulations very computationally expensive and often restrict the TFM to small scale 2D simulations. Alternative modelling approaches such as the Dense Discrete Phase Model (Popoff and Braun 2007) and the filtered Two Fluid Model (Igci, Andrews et al. 2008) are currently under development to also allow for the simulation of cases with fine powders and fast kinetics, but the standard TFM is likely to form the foundation of fluidized bed reactor modelling for many years into the future.

Just like the grid dependence behaviour of the TFM depends greatly on the flow conditions simulated, practical experience has shown other factors such as the wall interactions to also depend strongly on the flow conditions. This is an important observation because fluidized bed reactors can be designed to operate in a wide range of different flow regimes depending on the characteristics of the solid material and the desired reaction. For example, the classic work of Bi and Grace (Bi and Grace 1995) distinguishes between batch operation (typical bubbling or turbulent fluidization) and vertical transport (typical for the riser of a circulating fluidized bed), also identifying different flow regimes within each of these two categories.

TFM simulations of the carbonator in a potassium looping process for post combustion CO_2 capture (more information about this process can be found in (Samanta, Zhao et al. 2011)) will be employed to illustrate one flow regime where simulations are highly sensitive to poorly understood model coefficients (the wall friction and particle restitution coefficient). This will henceforth be termed the "example study". Subsequently, a more generic study of the impact of these two model coefficients under different flow conditions will be made. This will be termed the "generic study".

MODEL DESCRIPTION

The standard TFM equation set is employed with different drag closure laws for the example study (potassium looping) and the generic study (broad study across different flow regimes).

Conservation equations

In all cases, the fundamental conservation equations for mass, momentum and species were solved. Mass was conserved as follows:

$$\frac{\partial}{\partial t}\left(\alpha_g \rho_g\right)+\nabla\cdot\left(\alpha_g \rho_g \vec{v}_g\right)=\alpha_g S_g \quad (1)$$

$$\frac{\partial}{\partial t}\left(\alpha_s \rho_s\right)+\nabla\cdot\left(\alpha_s \rho_s \vec{v}_s\right)=0 \quad (2)$$

The source term for the gas phase equation (right hand term in (**1**) is included to account for mass transfer due to the heterogeneous reaction. Mass changes in the solids phase are neglected because these changes would be insignificant relative to the total mass of the solids.

Momentum conservation for the gas phase is written as

$$\frac{\partial}{\partial t}\left(\alpha_g \rho_g \vec{v}_g\right)+\nabla\cdot\left(\alpha_g \rho_g \vec{v}_g \vec{v}_g\right)=-\alpha_g \nabla p+\nabla\cdot\bar{\bar{\tau}}_g+\alpha_g \rho_g \vec{g}+K_{sg}\left(\vec{v}_s-\vec{v}_g\right)+S_g^{\vec{v}} \quad (3)$$

and for the solids as

$$\frac{\partial}{\partial t}\left(\alpha_s \rho_s \vec{v}_s\right)+\nabla\cdot\left(\alpha_s \rho_s \vec{v}_s \vec{v}_s\right)=-\alpha_s \nabla p-\nabla p_s+\nabla\cdot\bar{\bar{\tau}}_s+\alpha_s \rho_s \vec{g}+K_{gs}\left(\vec{v}_g-\vec{v}_s\right) \quad (4)$$

Species are also conserved for the gas phase.

$$\frac{\partial}{\partial t}\left(\alpha_g \rho_g Y_{g,i}\right)+\nabla\cdot\left(\alpha_g \rho_g \vec{v}_g Y_{g,i}\right)=\nabla\cdot\alpha_g \vec{J}_{g,i}+\alpha_g S_{g,i} \quad (5)$$

No energy conservation was considered under the assumption of isothermal reactor operation.

Closure relations

The conservation equations need to be closed by additional modelling.

Interphase momentum exchange

The drag laws governing the interphase momentum exchange ($K_{gs}=K_{sg}$ in (**3**) and (**4**)) were different for the two studies considered. For the example study, the correlation from Wen and Yu (Wen and Yu 1966) was used, while the more generic Syamlal and O'Brien drag law (Syamlal, Rogers et al. 1993) was implemented for the generic study. These are fairly standard selections in the literature.

Solids stresses

Solids stresses were modelled using the well documented kinetic theory of granular flows (KTGF) (Jenkins and Savage 1983, Lun, Savage et al. 1984, Gidaspow, Bezburuah et al. 1992, Syamlal, Rogers et al. 1993). In the KTGF analogy, the random motion of granular particles is put in analogy to the random motion of gas molecules where the kinetic theory of gasses is applied. This analogy allows the determination of fluid properties for the particulate phase by accounting for the inelasticity of the particles. The granular temperature is a measure of the energy contained in random particle motion and is conserved as follows:

$$\frac{3}{2}\left[\frac{\partial}{\partial t}\left(\alpha_s \rho_s \Theta_s\right)+\nabla\cdot\left(\alpha_s \rho_s \vec{v}_s \Theta_s\right)\right]=\left(-p_s \bar{\bar{I}}+\bar{\bar{\tau}}_s\right):\nabla\vec{v}_s+\nabla\cdot\left(k_{\Theta_s}\nabla\Theta_s\right)-\gamma_{\Theta_s}+\phi_{gs} \quad (6)$$

On the right hand side of the equation, the terms represent the generation of granular temperature via the solids stress tensor, granular temperature conductivity (Gidaspow, Bezburuah et al. 1992), dissipation of energy due to inelastic collisions (Lun, Savage et al. 1984) and the energy exchange between the gas phase and the random motions of the particles (Gidaspow, Bezburuah et al. 1992).

The granular temperature is subsequently used to calculate values of the solids viscosity which is used in the solids stress tensor. Bulk viscosity (Lun, Savage et al. 1984) and the three components of shear viscosity,

collisional (Gidaspow, Bezburuah et al. 1992, Syamlal, Rogers et al. 1993), kinetic (Gidaspow, Bezburuah et al. 1992) and frictional (Schaeffer 1987), were considered in the calculations.

Normal stresses modelled according to the solids pressure are calculated according to (Lun, Savage et al. 1984). The radial distribution function which is a measure of the average distance between particles is a central concept in the KTGF and is calculated according to (Ogawa, Unemura et al. 1980).

Reaction kinetics description

Due to the novelty of the potassium looping CO_2 capture process simulated in the example study, a sufficiently generic description of reaction kinetics specifically formulated for implementation into numerical models is not yet available from a single source. Therefore, the approach used in this paper uses insights from different works studying the kinetics of the carbonation reaction:

$$CO_2 + H_2O + K_2CO_3 \rightarrow 2KHCO_3$$

A simple reaction kinetics description where the rate is dependent only on the CO_2 concentration and the volume fraction of solids was used by (Chalermsinsuwan, Piumsomboon et al. 2010).

$$R^H = k_1 \alpha_s C_{CO_2} \tag{7}$$

This formulation is easy to implement in the code, but the reaction rate constant (taken as $k_1 = 1.95\ \mathrm{s}^{-1}$ in this case) was derived from a parallel plate reactor (not the real fluidized bed application studied here) and it was not expressed as a function of temperature.

Another research group studied the kinetics of the carbonation reaction by collecting CO_2 breakthrough data from a packed reactor and fit a deactivation model to this data (Park, Sung et al. 2006). The deactivation model produced a good fit and described how the material in their study was deactivated over time due to the diffusion resistance from a dense product layer forming on its outside. This deactivation process occurred on a rather long timescale (~1h in the experiments conducted) and will therefore not be significant in real applications where the particle residence time is in the order of seconds or minutes. The deactivation model used was also derived in terms of variables like the gas-solid contact time and the feed rate to the packed bed which is not suitable for implementation into a CFD model.

Therefore, it was assumed that the deactivation caused by the product layer formation is not significant and the rate is exclusively controlled by the kinetics. The aforementioned work (Park, Sung et al. 2006) determined a reaction rate constant as a function of time, but it was expressed in rather unconventional units (m^6/(kg.kmol.min)) as follows:

$$k_b = 1.191 \times 10^5 \exp\left(\frac{-7.544}{RT}\right) \tag{8}$$

Here, R is the universal gas constant expressed in kcal/(K.mol) and T is the temperature in Kelvin. In order to be useful for numerical modelling, however, this reaction rate constant has to be converted to a more standard form with the units of s^{-1}. This was done as follows:

In the experimental work (Park, Sung et al. 2006), this reaction rate constant was used in a 1D species conservation equation through the packed bed:

$$-Q_g \frac{dC_{CO_2}}{dw} = k_b C_{H_2O} C_{CO_2} \tag{9}$$

Here, Q_g is the volumetric flow rate of the feed gas and w is the weight of solids in the bed. In order to be useful for implementation into the CFD model, however, this equation has to be written in a dC_{CO_2}/dt form. This can be done through manipulation using the chain rule:

$$-Q_g \frac{dC_{CO_2}}{dw} = -Q_g \frac{dC_{CO_2}}{dt}\frac{dt}{dw} = -Q_g \frac{dC_{CO_2}}{dt}\frac{dt}{dV}\frac{dV}{dw} = -Q_g \frac{dC_{CO_2}}{dt}\frac{\alpha_g}{Q_g}\frac{1}{\alpha_s \rho_s} \tag{10}$$

(9) can now be rewritten in the desired form:

$$-\frac{dC_{CO_2}}{dt} = \left(\frac{k_b C_{H_2O} \rho_s}{\alpha_g}\right) \alpha_s C_{CO_2} \tag{11}$$

Here, the bracketed term represents the rate constant in the correct form with the units of s^{-1} as written in (7). (7) therefore implicitly assumes that the reaction rate is independent of the water vapour concentration, but this was proven not to be the case in (Park, Sung et al. 2006) where a first order dependency was observed. This work will therefore use a rate equation dependent on both the water vapour and CO_2 molar concentrations.

In addition, another work (Sharonov, Okunev et al. 2004) also observed an inverse proportionality between the reaction rate and the particle diameter. This is a well-known relationship implying that the reaction occurs on the surface of each particle and that smaller particles would present a larger combined surface area per unit volume than larger particles according the ratio between particle surface area and volume $(6/d_s)$.

The final rate equation will therefore be written in the form:

$$-\frac{dC_{CO_2}}{dt} = \frac{6}{d_p} \alpha_s k C_{H_2O} C_{CO_2} \tag{12}$$

In order to arrive at the correct expression for the reaction rate constant, the particle density and particle surface area per volume ratio have to be taken into account:

$$k = \frac{k_b \rho_s d_p}{6 \alpha_g} \tag{13}$$

Taking into account that the particle density was 2394 kg/m^3, the particle diameter was 401.67 µm and the bed void fraction was 0.475 in the experiments (Park, Sung et al. 2006), (13) can be rewritten as follows where the reaction rate constant has the units of (m^3/kmol).(m/s):

$$k = 669.75 \exp\left(\frac{-7.544}{RT}\right) \tag{14}$$

For the generic study, the simple hypothetical reaction rate description given below was used in order to convert species A into species B with a 1:1 stoichiometric ratio. Species A and B had the same material properties in order to ensure that the reaction would not have any influence on the hydrodynamics.

$$-\frac{dC_A}{dt} = 0.25\alpha_s x_A \qquad (15)$$

Geometry and meshing

The riser in the example study was modelled according to the specifications provided in (Yi, Jo et al. 2007). The total length of the riser was 6 m with an inner diameter of 2.5 cm. The lower 0.45 m of the riser was a mixing zone with a wider inner diameter of 3.5 cm which narrowed to 2.5 cm at a height of 0.6 m. 2.5 mm cubical cells were used in the mesh, resulting in a cell size roughly 25 times the particle size. A limited number of computationally expensive simulations were also performed on a mesh with 1.25 mm cells which resulted in 1.7 million cells in the domain.

Simulations for the generic study were carried out on a simple 2D planar geometry meshed with 2.5 mm cells which were also about 13 times the particle size. Five different geometries were studied both under batch (Table 1) and vertical transport (Table 2) operation where the total volume of the domain, the total gas flow through the domain and the total amount of solids within the domain was kept constant between runs as the aspect ratio was varied over a large range.

Table 1: Dimensions and fluidization velocity of the batch operation cases in the generic study.

Width (m)	Height (m)	Fluidization velocity (m/s)
2.4	0.3	0.1
1.2	0.6	0.2
0.6	1.2	0.4
0.3	2.4	0.8
0.15	4.8	1.6

Table 2: Dimensions and fluidization velocity of the vertical transport cases in the generic study.

Width (m)	Height (m)	Fluidization velocity (m/s)
0.600	1.200	1.600
0.424	1.697	2.263
0.300	2.400	3.200
0.212	3.394	4.525
0.150	4.800	6.400

Boundary conditions

The lower face of the geometry in the example study was specified as a velocity inlet, injecting gas at a velocity of 1.02 m/s and solids at a velocity of 0.0209 m/s and a volume fraction of 0.2. The gas stream consisted of 9.72% CO_2, 19% H_2O and the balance N_2 (on a molar basis). These specifications resulted in a gas superficial velocity of 2 m/s in the narrower 2.5 cm top section of the riser and a solids flux of 15 kg/m^{2}s. These were the conditions reported for the 11-17 hour operational period in (Yi, Jo et al. 2007).

For the generic study, the lower face of the geometry was also specified as a velocity inlet, injecting gas at the velocity specified in Table 1. The bed was initialized in such a way that the average solids volume fraction over the entire bed was 0.1. For the vertical transport cases in the generic study (Table 2), solids were also continuously injected over the velocity inlet at a volume fraction of 0.1 and a velocity which was 10% of the gas injection velocity.

The outlets of both geometries were specified as pressure outlets at atmospheric pressure. No-slip wall boundary conditions were specified for the gas phase, while partial slip boundary conditions (Johnson and Jackson 1987) were specified for the solids phase. It must be noted that this model has clear limitations and that improved methods are available (Li and Benyahia 2012, Schneiderbauer, Schellander et al. 2012). However, the Johnson and Jackson model remains the most popular method for accounting for partial slip of solids at walls in fluidized bed simulation studies and therefore merits further investigation. The specularity coefficient (ς in (16) and (17)) and the particle-wall restitution coefficient (e_{sw} in (17)) were varied between the different simulations carried out in this work.

$$\vec{\tau}_s = -\frac{\pi}{6}\sqrt{3}\varsigma\frac{\alpha_s}{\alpha_{s,\max}}\rho_s g_{0,ss}\sqrt{\Theta_s}\vec{U}_{s,\|} \qquad (16)$$

$$q_s = \frac{\pi}{6}\sqrt{3}\varsigma\frac{\alpha_s}{\alpha_{s,\max}}\rho_s g_{0,ss}\sqrt{\Theta_s}\vec{U}_{s,\|}\cdot\vec{U}_{s,\|} - \frac{\pi}{4}\sqrt{3}\frac{\alpha_s}{\alpha_{s,\max}}\left(1-e_{sw}^2\right)\rho_s g_{0,ss}\Theta_s^{3/2} \qquad (17)$$

For the example study, the temperature was fixed as a function of the reactor height in order to reproduce the temperature measurements taken in the experiments (Yi, Jo et al. 2007). The temperature (T) was fixed as a function of the height (h) through the following fourth-order polynomial:

$$T = -0.2073h^4 + 4.4354h^3 - 26.619h^2 + 45.941h + 353.15$$

No energy conservation was included in the bubbling fluidized bed simulations.

Material properties

Material properties for the gas and solids phases are given in Table 3 and Table 4. For the example study, the solids density was calculated from the given bulk density of 1100 kg/m^3 (Yi, Jo et al. 2007) assuming a solids volume fraction of 0.6 under packing.

Table 3: Material properties for the example study.

Gas density:	Ideal gas law
CO_2 viscosity:	4.68E-8T+1.00E-6 kg/(m.s)
H_2O viscosity:	3.42E-8T-3.75E-7 kg/(m.s)
N_2 viscosity:	4.32E-8T+4.94E-6 kg/(m.s)
Solids density:	1833 kg/m^3
Particle size:	98 µm

Table 4: Material properties for the generic study.

Gas density:	0.3 kg/m^3 (species A & B)
Gas viscosity:	4E-5 kg/(m.s) (species A & B)
Solids density:	2500 kg/m^3
Particle size:	200 µm
Minimum fluidization velocity:	0.0184 m/s

RESULTS AND DISCUSSION

This section will be divided in two parts discussing results from the example and generic studies.

Example study

The sensitivity of this narrow riser simulation to unknown model coefficients; the specularity coefficient, the particle-wall restitution coefficient and the particle-particle restitution coefficient, was evaluated by means of a central composite design (Montgomery 2001). This is a form of experimental design (also applicable to simulation experiments) where the response of specific dependent variables to changes in various independent

variables can be easily assessed, accurately quantified and visualized. The three aforementioned model coefficients were taken as the independent variables and simulation behaviour was quantified by means of two dependent variables: the overall pressure drop, which is equivalent to the holdup, and the overall degree of CO_2 absorption.

The central composite design consisted of 16 simulation experiments, filling the three dimensional parameter space with the reactor performance resulting from each specific set of model coefficients. Results will be displayed in two ways: an analysis of variance (ANOVA) and response surfaces of dependent variables to changes in various independent variables. The ANOVA will be used to quantify the significance of the independent variables (i.e. identify the model coefficients which had a statistically significant influence on the simulation behaviour).

The significance of factors will be defined by the p-value which is an indication of the probability of the observed effect to result purely by random chance. If this value becomes small $(p < 0.05)$, the effect is said to be significant because the probability of it arising from pure chance is fairly small. A value of $p < 0.01$ is generally regarded as highly significant. The p-value is calculated from the F-test which weighs the amount of explained variance in the design against the amount of unexplained variance (experimental error, rounding error, averaging error, data not fitting the second order model etc.). This ratio can then be evaluated as a p-value to decide whether the variance is caused by a significant effect or is simply random.

Table 5: ANOVA table summarizing the response of the total pressure drop and the degree of CO_2 absorption to changes in the three unknown model coefficients under investigation: the specularity coefficient (S), the particle-particle restitution coefficient (PP) and the particle-wall restitution coefficient (PW). Significant factors are shown in bold, while highly significant factors are shown in bold italics. The factors are denoted by S (specularity coefficient), H (particle-wall restitution coefficient) and d (particle-particle restitution coefficient). Different effects are indicated by L (linear), Q (quadratic) and by (interaction).

Effect	Pressure drop		CO_2 absorption	
	SS (%)	p-value	SS (%)	p-value
S(L)	***36.12***	***0.0006***	***37.38***	***0.0032***
S(Q)	**5.16**	**0.0453**	3.02	0.2271
PP(L)	***32.29***	***0.0007***	***31.63***	***0.0048***
PP(Q)	4.54	0.0561	2.78	0.2442
PW(L)	4.20	0.0635	6.22	0.1016
PW(Q)	1.26	0.2605	1.71	0.3501
S(L) by PP(L)	***15.56***	***0.0047***	**10.74**	**0.0441**
S(L) by PW(L)	0.11	0.7222	0.00	0.9936
PP(L) by PW(L)	0.13	0.7009	0.02	0.9083
Error	4.88		10.00	
Total	100.00		100.00	

The relative variance explained by each factor will also be given as the percentage of the total sum of squares (SS). The total sum of squares is the sum of all the squared distances between the various data points and the mean. A larger total sum of squares implies that the data are scattered wide around the mean and there is a lot of variance in the design. This measure will give an indication of the importance of significant effects relative to each other. The ANOVA results for the riser simulation are given in Table 5.

It is clear from the data in Table 5 that changes in the specularity coefficient and the particle-particle restitution coefficient had the greatest impact on the results, while the effect of particle-wall restitution coefficient was not statistically significant. This is in line with results from an earlier study on the parametric sensitivity of riser simulations (Cloete, Amini et al. 2011).

However, the most important result from this central composite design is the magnitude of the variations in overall pressure drop and CO_2 absorption caused by changes in the unknown model coefficients. This large variation is shown in Figure 1.

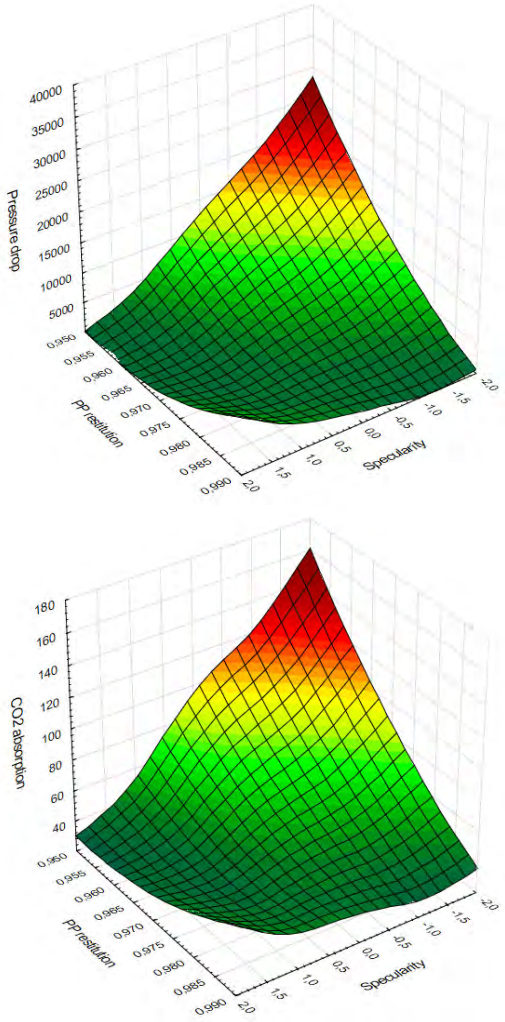

Figure 1: Response of the total pressure drop (Pa) and the CO2 absorption (%) in response to changes in the specularity coefficient and the particle-particle restitution coefficient. Note that the specularity coefficient is given in coded variables (c) where the actual specularity coefficient is given by: $\varsigma = 0.002 \times 2^c$.

Firstly, it must be pointed out that the maximum values in Figure 1 (at the lowest values of the specularity and particle-particle restitution coefficients) can be

misleading because it is an extrapolation of a very sharp gradient. For example, the CO_2 absorption cannot be more than 100%, but the extrapolated value projects an absorption of 160% at the lowest specularity and particle-particle restitution coefficients observed in the simulation.

When looking at results from the simulations, a specularity coefficient of 0.001 (coded variable of -1) and a particle-particle restitution coefficient of 0.96 returned a pressure drop of 12.5 kPa and 89.2% CO_2 absorption, while a specularity coefficient of 0.004 (coded variable of 1) and a particle-particle restitution coefficient of 0.98 returned a pressure drop of 1.3 kPa and 34.7% CO_2 absorption. It is therefore clear that this relatively small variation in model coefficients caused almost an order of magnitude difference in the solids holdup in the riser.

The reason for this large influence is the non-linear influences that cluster formation has on riser performance. Cluster formation can be a self-reinforcing phenomenon since the presence of clusters creates the large velocity gradients necessary to separate free particles from streamlines so that they join into the bulk of the cluster (Cloete, Johansen et al. 2015). This non-linear nature of clustering causes the large difference in riser hydrodynamics shown in Figure 2.

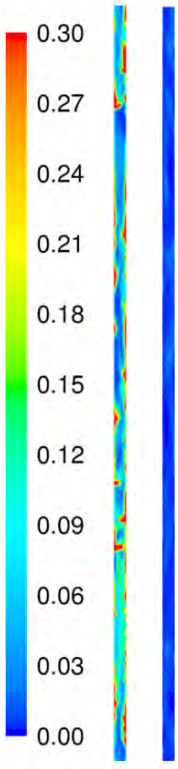

Figure 2: (On the left) Instantaneous volume fraction profiles in identical locations in the riser for the case with a specularity coefficient of 0.001 and a particle-particle restitution coefficient of 0.96 (left) and the case with a specularity coefficient of 0.004 and a particle-particle restitution coefficient of 0.96 (right).

Lower particle-particle restitution coefficients are beneficial to clustering due to the increased dissipation of granular temperature (and the associated reduction in granular pressure) in denser regions. Lower specularity coefficients are beneficial to clustering due to the free slip of denser clusters across smoother walls without being broken up by excessive shear forces. It appears evident that cluster formation is triggered over a very small range of these unknown model coefficients and causes large differences in riser behaviour after being triggered.

In order to assess the influence of the grid size on these phenomena, three computationally expensive simulations were completed on a mesh which was refined via hanging node adaption. Interestingly, the clustering was triggered at significantly lower specularity and particle-particle restitution coefficients than on the coarse mesh. This is counter-intuitive because finer meshes are normally more conducive to clustering. Finer meshes can resolve the high flow gradients around clusters, allowing free-flowing particles to deviate from the streamlines and join in the bulk of the cluster. It is expected that this trend is caused by the larger flow gradients resolved at the walls which can break up clusters more efficiently than on the coarser grid.

The three fine grid simulations were therefore carried out using a particle-particle restitution coefficient of 0.9 and specularity coefficients varying over a wide range of 0.01, 0.001 and 0.0001. The resulting match to pressure drop data from the experiment is given in Figure 3.

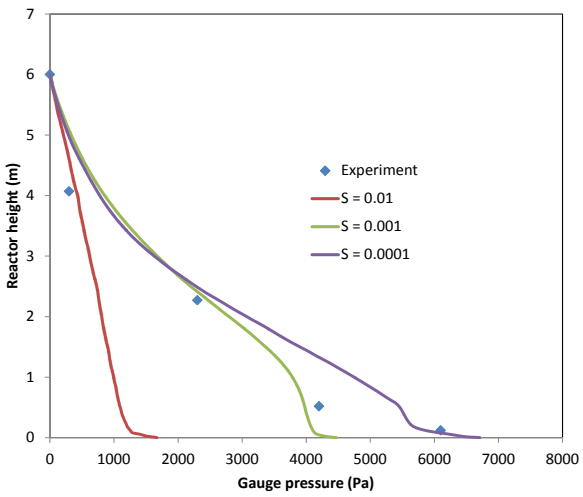

Figure 3: Model comparisons to axial pressure measurements (Yi, Jo et al. 2007) using different specularity coefficients (S) and a particle-particle restitution coefficient of 0.9.

It is shown that the simulations with a low specularity coefficient matched the experimental results well, but a higher specularity coefficient caused a situation where very little cluster formation was simulated and the solids holdup in the reactor was greatly under-predicted.

For the low specularity coefficient cases, a comparison was also made to species measurements at the outlet of the reactor. The simulation returned values around 70% CO2 capture at the outlet while the experimental measurements returned about 50% CO2 capture. This implies that the reaction rate constant in (14) is too high and will need refinement through dedicated experiments.

Generic study

The discussion will be split between the batch operation cases (Table 1) and the vertical transport cases (Table 2).

Batch operation cases

It can be expected that the large influence of unknown model coefficients on important model outputs observed in the previous section for the riser will be significantly reduced for dense fluidization. There are two main reasons for this observation.

Firstly, dense fluidized beds generally have larger diameters due to the fact that they have to employ smaller fluidization velocities. A larger diameter implies a smaller walls/volume ratio and therefore a smaller wall influence. In addition, the slower fluidization in

dense beds will result in smaller wall shear forces and therefore less of an influence on the overall reactor behaviour.

Secondly, dense fluidized beds, if solved on a sufficiently fine grid, will always display clustering or bubbling. The sudden transition from a situation of no clustering to a situation of significant clustering illustrated in Figure 2 can therefore not happen in dense fluidized beds.

As a result of these two factors, it is reasoned that dense fluidization can be simulated with a much larger degree of confidence than riser flow. This assumption was tested via the five cases outlined in Table 1.

Two main variables will be extracted to describe the macroscopic behaviour of the reactor: the pressure drop over the bottom 25% of each domain (an area filled with solids in all cases) and the reactor performance defined as the negative logarithm of the reactant mole fraction exiting the reactor unreacted.

The aim of using the $-\log(x_A)$ measure is to linearize the performance achieved by the reactor running a first order reaction. For example, if all other variables were kept constant, a reactor running a first order reaction would require twice the amount of residence time to achieve 99% conversion than to achieve 90% conversion. Hence, the reactor performance of a reactor achieving 99% conversion is $-\log(0.01)=2$ while the reactor performance of a reactor achieving 90% conversion is $-\log(0.1)=1$.

Firstly, the grid dependency behaviour of the dense fluidized bed cases must be evaluated. As shown in Figure 4 and Figure 5, the influence of different grid sizes on the reactor behaviour was fairly small, especially with regard to the pressure drop. For engineering applications, results derived from the 5 mm grid would be adequate, but the 2.5 mm grid was used in the remainder of this study.

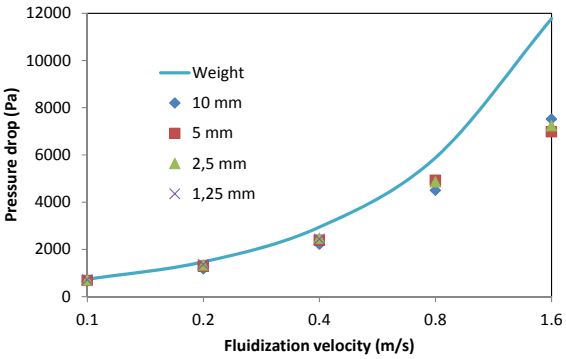

Figure 4: Pressure drop in the lower 25% of the reactor for the five different cases in Table 1 calculated using different cell sizes. The pressure drop related to the weight of the solids is also included for perspective.

The grid dependency effects displayed in Figure 4 and Figure 5 are small in comparison to that observed in the riser case where one refinement could cause a transition from fast fluidization to pneumatic transport, thereby completely changing the behaviour of the reactor.

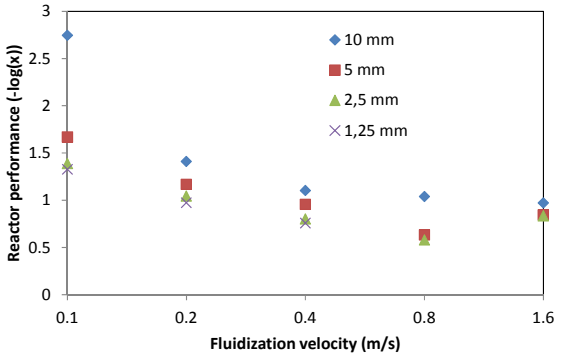

Figure 5: Reactor performance for the five different cases in Table 1 using different cell sizes.

Secondly, the effect of specularity coefficient was assessed with results presented in Figure 6 and Figure 7.

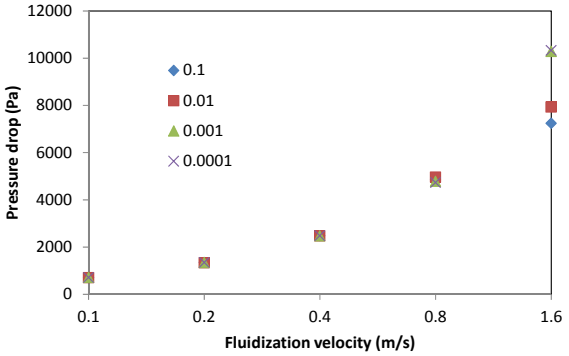

Figure 6: Pressure drop in the lower 25% of the reactor for the five different cases in Table 1 calculated using different specularity coefficients.

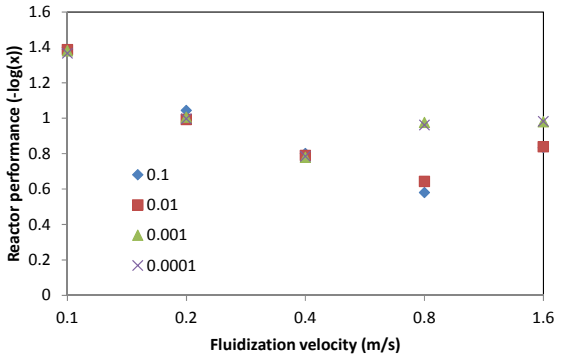

Figure 7: Reactor performance for the five different cases in Table 1 using different specularity coefficients.

It is clear that large changes in the specularity coefficient had no discernible impact on the model results for the cases with a fluidization velocity of 0.4 m/s and below. For the cases with a fluidization velocity of 0.8 m/s and 1.6 m/s, however, a significant difference in rector performance can be observed when transitioning from a specularity coefficient of 0.01 to a specularity coefficient of 0.001.

These geometries were only 30 and 15 cm in diameter respectively and therefore were subject to a significant degree of influence from the walls. As shown in Figure 8, this influence had a significant impact on the nature of the cluster formation in the fluidized bed.

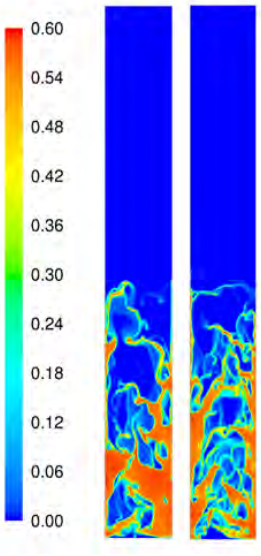

Figure 8: (On the left) Instantaneous volume fraction profiles for the case with a fluidization velocity of 0.8 m/s. The left-hand image is for a specularity coefficient of 0.01 and the right hand image is for a specularity coefficient of 0.001.

The hydrodynamic difference created by a change in the specularity coefficient from 0.01 to 0.001 is evident from Figure 8. When the specularity coefficient is lowered, falling solids near the wall create higher shear forces, leading to finer and more chaotic flow structures. It is clear from Figure 7 that these finer flow structures led to increased gas-solid contact and improved reactor performance (greater conversion).

Figure 6 shows, however, that this improved gas-solid contact was cancelled out to a certain degree in the 1.6 m/s fluidization velocity case by a more compacted bed in the lower reactor regions. This more compact bed reduced the quality of gas/solid contact in this region thereby countered the improved mass transfer effect of the finer flow structures to a certain degree. This is the reason why the specularity coefficient appears to have a larger influence on the reactor performance in the case with 0.8 m/s fluidization velocity than in the case with 1.6 m/s fluidization velocity.

Thirdly, the sensitivity of the dense fluidized bed simulations to changes in the particle-particle restitution coefficient was assessed. As shown in Figure 9 and Figure 10, the impact is again moderate at higher fluidization velocities and negligible at lower fluidization velocities.

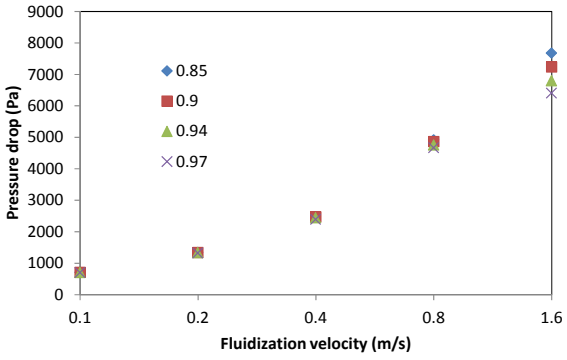

Figure 9: Pressure drop in the lower 25% of the reactor for the five different cases in Table 1 calculated using different particle-particle restitution coefficients.

For the reactor performance (Figure 10) all cases show a discernible impact of the highest particle-particle restitution coefficient (0.97). At this value, cluster formation was sufficiently suppressed to enhance gas-solid contact and thereby increase reactor performance. However, for particle-particle restitution coefficients around values that are usually employed (~0.9), the impact seems to be small.

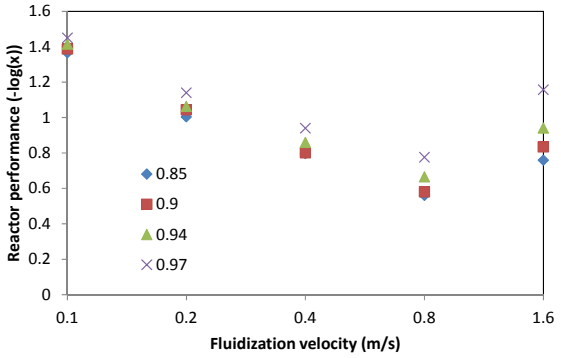

Figure 10: Reactor performance for the five different cases in Table 1 using different particle-particle restitution coefficients.

It is therefore clear that the sensitivity of dense fluidized bed simulations to changes in the two most important unknown model coefficients is much smaller than for the narrow riser case shown in Figure 1.

Vertical transport cases

For the vertical transport cases (Table 2), $-\log(x_A)$ was also used to evaluate the amount of conversion that takes place. However, the average volume fraction of the solids phase within the entire geometry was used as the hydrodynamic performance measure.

When varying the specularity coefficient it is observed (Figure 11) that there is a small effect on solid holdup at all velocities. The overall effect appeared to be too small to distinguish a clear trend on how the specularity coefficient influences the amount of solids in the riser. On the other hand, when evaluating the reactor performance (Figure 12), the effect of the specularity coefficient is highly significant at lower fluidization velocities, but almost disappears for the highest two velocities investigated.

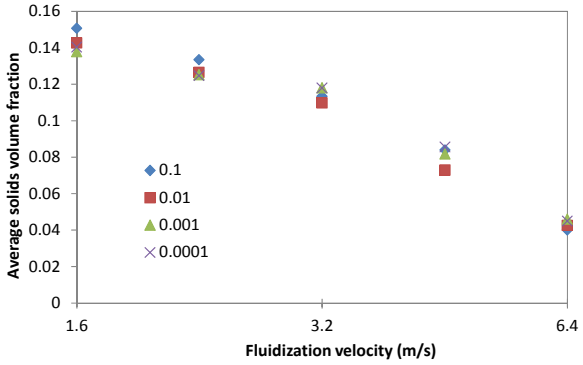

Figure 11: Average solid holdup for five different cases in Table 2 using different specularity coefficients.

Plots of the instantaneous solids volume fraction for different specularity coefficients aid in explaining these trends. Figure 13 shows such plots for the case with a fluidization velocity of 2.26 m/s, where the largest changes in reactor performance were observed. It is shown that at lower specularity coefficients there are streaks of falling solids near the walls. This is similar to what occurred in the dense fluidized bed and the resulting shear stresses cause finer flow structures to form. With an increase in the specularity coefficient, the amount of falling solids decrease and more distinct solids clusters form.

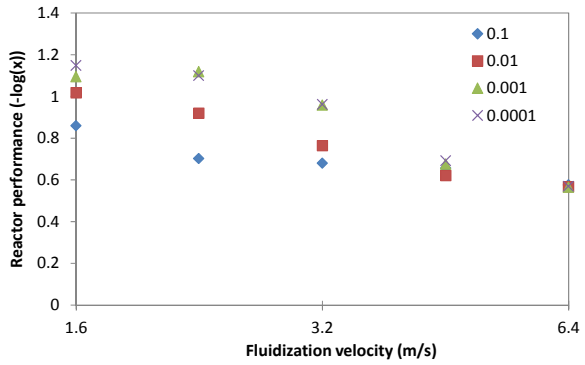

Figure 12: Reactor performance for five different cases in Table 2 using different specularity coefficients.

There are therefore two effects that influence the solid holdup as the specularity coefficient is decreased. Firstly, an increase in falling solids near the walls will tend to keep the solids in the riser column. On the other hand, the finer solid structures will be more easily transported from the column by the gas flow. The relatively small change in solid holdup with specularity coefficient observed in Figure 11 therefore shows that these two effects balance each other out over all fluidization velocities considered.

No sudden regime transitions as seen in the example study were observed. The complete lack of sensitivity of the faster cases to changes in the specularity coefficient is especially surprising considering the large influence of the wall in these cases. This result illustrates that the two effects described above effectively cancel each other out in narrow geometries and that a step change can only be expected when approaching the dilute transport regime where a sudden transition between smooth and clustered flow can be triggered.

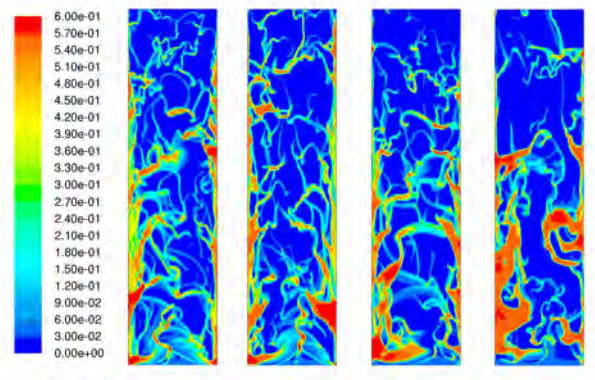

Figure 13: Instantaneous volume fraction profiles for the case with a fluidization velocity of 2.26 m/s. From left to right the specularity coefficients used are: 0.0001, 0,001, 0.01 and 0.1.

In the case of reactor performance, the finer flow structures at low specularity coefficients lead to better gas-solid contact, which explains the increase in conversion with a decrease in specularity coefficient observed in Figure 12.

Analyses of the solid holdup at different particle-particle restitution coefficients shows a clear trend of increased holdup with a decrease in the particle-particle restitution coefficient. This effect changes from moderate (13% increase) at low fluidization velocity to severe (113% increase) at high fluidization velocities. Clusters will form more readily at lower particle-particle restitution coefficients and there will be fewer fine solid structures that can easily be transported from the column.

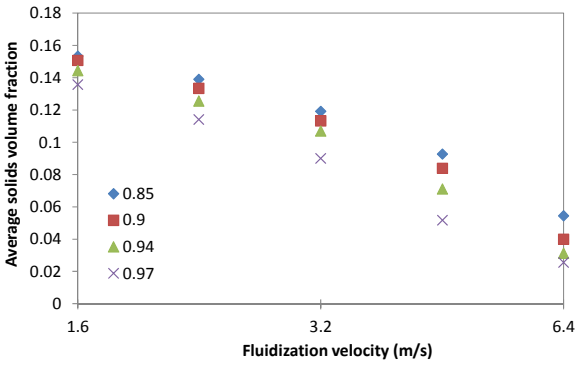

Figure 14: Average solid holdup for five different cases in Table 2 using different particle-particle restitution coefficients.

When assessing the effect on reactor performance (Figure 15), it is seen that, for lower fluidization velocities, the reactor performance increases at higher particle-particle restitution coefficients. This is due to better gas/solid contact in the finer flow structures that form. However, at faster fluidization velocities, the amount of solids present in the riser column decreases significantly at increased particle-particle restitution coefficients, limiting the conversion in the gas phase. Therefore, at fluidization velocities of 4.53 m/s and 6.4 m/s the effect on the reaction rate of increases in solid-gas contact and decreases in the amount of solids cancel each other almost exactly. This explains why changes in the particle-particle restitution coefficient have a negligible impact at faster fluidization velocities.

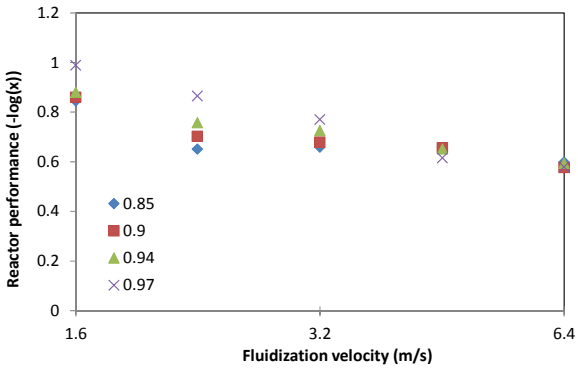

Figure 15: Reactor performance for five different cases in Table 2 using different particle-particle restitution coefficients.

CONCLUSION

The kinetic theory of granular flows commonly used in granular flow simulations involves a number of model coefficients which are difficult to determine accurately and therefore often used as tuning coefficients. These coefficients introduce a significant amount of uncertainty to fluidized bed simulations and can potentially have a large impact on model results.

This study investigated three such model coefficients: the specularity coefficient, the particle-wall restitution coefficient and the particle-particle restitution

coefficient. Of these coefficients, the specularity and particle-particle restitution coefficient were shown to have the greatest impact on model results.

The impact of these unknown model coefficients on simulation results depends strongly on the flow regime under which the simulations were carried out. A very narrow riser case showed large non-linear responses to changes in the specularity and particle-particle restitution coefficients as these coefficients triggered a regime change in the reactor. On the other hand, for bubbling, turbulent and fast fluidization where cluster formation is always present, such rapid regime changes were not observed.

For bubbling fluidization in wide reactors, the effect of these unknown coefficients can become negligible. This, combined with the fact that bubbling beds generally use larger particle sizes and slower reaction rates, makes such reactors much simpler to simulate than faster riser reactors. Even though rapid step changes were not observed for clustered flows in narrower geometries under faster fluidization, the influence of the unknown model coefficients did become increasingly significant, thereby introducing significant amounts of uncertainty into the simulation results.

ACKNOWLEDGEMENTS

The authors gratefully acknowledge the research funding received from the Research Council of Norway as well as the Notur supercomputing facilities used to carry out the expensive riser simulations in this paper.

REFERENCES

Bi, H. T. and J. R. Grace (1995). "Flow regime diagrams for gas-solid fluidization and upward transport." International Journal of Multiphase Flow **21**(6): 1229-1236.

Chalermsinsuwan, B., P. Piumsomboon and D. Gidaspow (2010). "A computational fluid dynamics design of a carbon dioxide sorption circulating fluidized bed." AIChE Journal **56**(11): 2805-2824.

Cloete, S., S. Amini and S. T. Johansen (2011). "A fine resolution parametric study on the numerical simulation of gas-solid flows in a periodic riser section." Powder Technology **205**(1-3): 103-111.

Cloete, S., S. T. Johansen and S. Amini (2015). "Grid independence behaviour of fluidized bed reactor simulations using the Two Fluid Model: Effect of particle size." Powder Technology **269**(0): 153-165.

Cloete, S., A. Zaabout, S. T. Johansen, M. Van Sint Annaland, F. Gallucci and S. Amini (2014). "The effect of frictional pressure, geometry and wall friction on the modelling of a pseudo-2D bubbling fluidized bed reactor." Powder Technology **Under review**.

Ellis, N., M. Xu, C. J. Lim, S. Cloete and S. Amini (2011). "Effect of Change in Fluidizing Gas on Riser Hydrodynamics and Evaluation of Scaling Laws." Industrial & Engineering Chemistry Research **50**(8): 4697-4706.

Gidaspow, D., R. Bezburuah and J. Ding (1992). Hydrodynamics of Circulating Fluidized Beds, Kinetic Theory Approach. 7th Engineering Foundation Conference on Fluidization 75-82.

Igci, Y., A. T. Andrews, S. Sundaresan, S. Pannala and T. O'Brien (2008). "Filtered two-fluid models for fluidized gas-particle suspensions." AIChE Journal **54**(6): 1431-1448.

Jenkins, J. T. and S. B. Savage (1983). "Theory for the rapid flow of identical, smooth, nearly elastic, spherical particles." Journal of Fluid Mechanics **130**: 187-202.

Johnson, P. C. and R. Jackson (1987). "Frictional-Collisional Constitutive Relations for Granular Materials, with Application to Plane Shearing." Journal of Fluid Mechanics **176**: 67-93.

Li, T. and S. Benyahia (2012). "Revisiting Johnson and Jackson boundary conditions for granular flows." AIChE Journal **58**(7): 2058-2068.

Lun, C. K. K., S. B. Savage, D. J. Jeffrey and N. Chepurniy (1984). "Kinetic Theories for Granular Flow: Inelastic Particles in Couette Flow and Slightly Inelastic Particles in a General Flow Field." Journal of Fluid Mechanics **140**: 223-256.

Montgomery, D. (2001). Design and Analysis of Experiments. New York, John Wiley and Sons.

Ogawa, S., A. Unemura and N. Oshima (1980). "On the Equation of Fully Fluidized Granular Materials." Journal of Applied Mathematics and Physics **31**: 483.

Park, S.-W., D.-H. Sung, B.-S. Choi, J.-W. Lee and H. Kumazawa (2006). "Carbonation kinetics of potassium carbonate by carbon dioxide." Journal of industrial and engineering chemistry **12**(4): 522-530.

Popoff, B. and M. Braun (2007). A Lagrangian Approach to Dense Particulate Flows. 6th International Conference on Multiphase Flow. Leipzig, Germany.

Samanta, A., A. Zhao, G. K. H. Shimizu, P. Sarkar and R. Gupta (2011). "Post-Combustion CO2 Capture Using Solid Sorbents: A Review." Industrial & Engineering Chemistry Research **51**(4): 1438-1463.

Schaeffer, D. G. (1987). "Instability in the Evolution Equations Describing Incompressible Granular Flow." Journal of Differential Equations **66**: 19-50.

Schneiderbauer, S., D. Schellander, A. Löderer and S. Pirker (2012). "Non-steady state boundary conditions for collisional granular flows at flat frictional moving walls." International Journal of Multiphase Flow **43**(0): 149-156.

Sharonov, V., A. Okunev and Y. Aristov (2004). "Kinetics of carbon dioxide sorption by the composite material K2CO3 in Al2O3." Reaction Kinetics and Catalysis Letters **82**(2): 363-369.

Syamlal, M., W. Rogers and T. J. O'Brien (1993). MFIX Documentation: Volume 1, Theory Guide. Springfield, National Technical Information Service.

Taghipour, F., N. Ellis and C. Wong (2005). "Experimental and computational study of gas-solid fluidized bed hydrodynamics." Chemical Engineering Science **60**(24): 6857-6867.

Wen, C. Y. and Y. H. Yu (1966). "Mechanics of Fluidization." Chemical Engineering Progress Symposium Series **62**: 100-111.

Yi, C.-K., S.-H. Jo, Y. Seo, J.-B. Lee and C.-K. Ryu (2007). "Continuous operation of the potassium-based dry sorbent CO2 capture process with two fluidized-bed reactors." International Journal of Greenhouse Gas Control **1**(1): 31-36.